ADVANCED OPTICAL MATERIALS
www.advopticalmat.de

Enhanced Light Emission Performance of Mixed Cation Perovskite Films—The Effect of Solution Stoichiometry on Crystallization

Fangzhou Liu, Xinshun Qin, Bing Han, Christopher C. S. Chan, Chao Ma, Tik Lun Leung, Wei Chen, Yanling He, Ivor Lončarić, Luca Grisanti, Juraj Ovčar, Željko Skoko, Yingli Shi, Francis Chi Chung Ling, Md Rashedul Huqe, Juan Antonio Zapien, Shixun Wang, Chun-Jen Su, U-Ser Jeng, Kam Sing Wong, Alan Man Ching Ng, Meng Gu, Jasminka Popović,* and Aleksandra B. Djurišić**

The performance of quasi-2D perovskite light emitting diodes (LEDs) with mixed small cations, cesium and formamidinium (FA), is significantly affected by their ratio. The best devices obtained for Cs:FA ratio of 1:1 exhibit a maximum external quantum efficiency (EQE) of 12.1%, maximum luminance of 15 070 cd m^{-2} and maximum current efficiency of 46.1 cd A^{-1}, which is significantly higher (about 3 times) compared to devices with FA only (maximum EQE of 4.1%, maximum luminance of 4521 cd m^{-2}) and Cs-only (maximum EQE of 4.0%, maximum luminance of 4886 cd m^{-2}). The photoluminescence quantum yield of the Cs:FA 1:1 sample is similarly enhanced, 21.3% compared 5.4% and 6%, for FA-only and Cs-only samples, respectively. It can be observed that the Cs:FA ratio significantly affects the crystallization of the perovskite, with the optimal 1:1 ratio resulting in the formation of tetragonal $Cs_{0.5}FA_{0.5}PbBr_3$ phase (different from cubic $FAPbBr_3$ and orthorhombic $CsPbBr_3$) with pronounced preferential orientation as well as a significant reduction in the trap density, which leads to a substantial improvement in the light-emitting performance.

1. Introduction

Optical properties and light emission from halide perovskites for possible light-emitting applications have been intensively studied in recent years.[1–37] Among different halide perovskite materials, layered 2D/quasi-2D perovskites have been attracting increasing attention due to their higher exciton binding energies, increased ambient and thermal stability, wider tunability, and the possibility of radiative recombination enhancement by tuning the film composition to achieve efficient energy transfer from higher bandgap to lower bandgap quasi-2D perovskites.[1] Different from common 3D halide perovskites with a formula ABX_3, quasi-2D Ruddlesden–Popper perovskites (RPP) have a

F. Liu, X. Qin, T. L. Leung, W. Chen, Y. He, Y. Shi, F. C. C. Ling, A. B. Djurišić
Department of Physics
The University of Hong Kong
Pokfulam Road, Hong Kong, Hong Kong SAR, China
E-mail: dalek@hku.hk

B. Han, M. Gu
Department of Materials Science and Engineering
Southern University of Science and Technology
No. 1088, Xueyuan Road, Shenzhen, Guangdong 518055, China
E-mail: b.han@pku.edu.cn

C. C. S. Chan, C. Ma, K. S. Wong
Department of Physics
The Hong Kong University of Science and Technology
Clearwater Bay, Hong Kong, Hong Kong SAR, China

Y. He, A. M. C. Ng
Department of Physics
Southern University of Science and Technology
No. 1088, Xueyuan Road, Shenzhen, Guangdong 518055, China

The ORCID identification number(s) for the author(s) of this article can be found under https://doi.org/10.1002/adom.202100393.

DOI: 10.1002/adom.202100393

I. Lončarić, L. Grisanti, J. Ovčar, J. Popović
Ruđer Bošković Institute
Bijenička 54, Zagreb 10000, Croatia
E-mail: jpopovic@irb.hr

Ž. Skoko
Department of Physics
Faculty of Science
University of Zagreb
Bijenička 32, Zagreb 10000, Croatia

M. R. Huqe, J. A. Zapien
Department of Materials Science and Engineering
City University of Hong Kong
83 Tat Chee Avenue, Kowloon, Hong Kong SAR, China

S. Wang
Department of Materials Science and Engineering
Centre for Functional Photonics (CFP)
City University of Hong Kong
83 Tat Chee Avenue, Kowloon, Hong Kong SAR, China

C.-J. Su, U.-S. Jeng
National Synchrotron Radiation Research Center
Hsinchu Science Park, Hsinchu 30076, Taiwan

U.-S. Jeng
Department of Chemical Engineering
National Tsing Hua University
Hsinchu 30013, Taiwan

 © 2021 Wiley-VCH GmbH

general formula $R_2A_{n-1}B_nX_{3n+1}$, where R^+ is the bulky amine spacer cation, A^+ is a small organic or alkali metal cation, B^{2+} is a divalent metal cation, X^- is a halide anion, and n is the number of perovskite layers.[1] It has been shown that the coexistence of quasi-2D and 3D perovskite results in a significant enhancement of the emission efficiency compared to pure 3D perovskites, as well as improved environmental stability.[2] Large organic cations also serve to passivate defects in grain or domain boundaries.[6] However, despite these advantages, the achieved efficiencies of quasi-2D perovskite-based LEDs have been limited by nonoptimized distributions of different n phases, and increased defects at surface or grain boundaries.[7]

The common approaches to increasing the efficiency of quasi-2D LEDs include optimizing the film composition or deposition to optimize the distribution of quasi-2D phases with different n to achieve efficient funnelling,[2,4,5,6,10,12] using post-treatments to remove excess spacer cations,[8] optimizing the device architecture,[3,9] or using additives to passivate defects.[7,15] The optimization of the film composition would typically involve the optimization of the solution stoichiometry, as well as the choices of spacer cations R^+ and small cations B^+. Various spacer cations have been reported to date, and common choices involve alkyl chain spacers such as butylammonium (BA), which yielded efficiencies ranging from ≈7% to 16%,[8,9,12,13,18] as well as aromatic spacers such as phenethylamine (PEA), which yielded efficiencies in the range %7–15%.[3–7] Among possible small cations A^+, all three possible choices, namely Cs,[2,8,9,11] formamidinium (FA),[3,6,12] and methylammonium (MA),[4,5,18] have been reported. Recently, the use of mixed cations has been proposed as a feasible method to control the crystallization and consequently film composition and emission efficiency. Both spacer cation[12] and small cation[10,14,19–27] mixing has been investigated. The small cation mixing approach is particularly interesting since it is applicable to both 3D and quasi-2D perovskite emitters. Different combinations of small cation mixtures have been reported, such as MA-ethylammonium,[20] MA-Cs,[21,25–27] and Cs-FA,[10,14,19,22–24] and the use of mixed cations for both 3D and quasi-2D perovskite based films and devices can result in significant performance improvements compared to the cases with single-cations. However, the reported current efficiencies for 3D perovskite based devices with mixed cations are typically below 15 cd A^{-1},[23–25] while higher current efficiencies (≈17–54 cd A^{-1}) have been reported in quasi-2D perovskite based devices.[10,19–21]

In quasi-2D perovskites, the use of mixed small cations was reported to result in improved film quality, changes in the film composition (the suppression of phases with small n number), and reduced efficiency roll-off at higher bias[10,14,19] due to supressed Auger recombination.[14] For example, the improvement in performance for CsFA-based quasi-2D perovskite was attributed to improved film quality and lower roughness.[10] The incorporation of FA was also found to suppress the formation of undesirable low n phases.[10,14] However, the effect of small cation mixing on the crystal structure of the mixed phase has not been explored in detail, and how this affect the light emission and LED performance is mostly unknown. Nevertheless, there are indications that the performance enhancement due to the use of mixed small cations has additional effects beyond the suppression of the formation of low n phases and reduced surface roughness. This is particularly important in Cs-containing devices, where multiple phases of cesium lead bromide are possible, which can lead to complex interplay between sample crystallinity and light-emitting performance. For example, it has been reported that the optimized concentration of spacer cation can supress the formation of unfavourable phase of Cs_4PbBr_6 in the quasi-2D perovskite $PEA_2(Cs_{0.5}FA_{0.5})_{n-1}Pb_nBr_{3n+1}$, resulting in increased light emission for optimized composition.[19] In this case, while another possible crystal phase of cesium lead bromide, namely $CsPb_2Br_5$, has also been detected in $PEA_2(Cs_{0.5}FA_{0.5})_{n-1}Pb_nBr_{3n+1}$,[19] the detailed implications of its formation on the light emission have not been explored. It has been pointed out that the presence of additional crystal phases, such as $CsPb_2Br_5$ and Cs_4PbBr_6, could affect the defect densities and photoluminescence quenching, and these two crystal phases play fundamentally different role in the luminescence of the perovskite emitters. Different synthesis conditions can result in different phases of cesium lead bromide, including $CsPbBr_3$, $CsPb_2Br_5$, and Cs_4PbBr_6. These phases can readily transform into each other, and the inclusions of one phase can form within other phases,[32,37] and the origin of luminescence of $CsPb_2Br_5$ has been controversial.[34–36] Despite these controversies, $CsPb_2Br_5$ phase in particular has been attracting growing attention recently,[28–37] and there have been many reports on the efficient $CsPb_2Br_5$-based[29] and $CsPbBr_3$-$CsPb_2Br_5$-based LEDs.[28,30–32] It is well known that perovskite materials in general are extremely sensitive to the preparation conditions, leading to different behaviors observed in literature reports. These differences in behavior are likely to occur due to differences in native defects, which can result in luminescence quenching.[34] Nevertheless, the existing reports with enhanced light emission in samples containing $CsPb_2Br_5$ indicates that the improved optical properties can be achieved for optimized samples, and thus it is worth investigating the relationship between the film structure (including the presence of different cesium lead bromide phases), its optical properties, and the device performance.

Here, we present a detailed investigation into the crystal structure and optical properties of mixed small cation quasi-2D LEDs. We demonstrate that the ratio of FA and Cs has a significant effect on the structural features of crystalline phases within the thin films, its light emission properties and consequently the device performance. LEDs based on $Cs_{0.5}FA_{0.5}$ emitters clearly outperform devices with both pure Cs and pure FA-based perovskites. The films were prepared using a solution with stoichiometry $n = 4$, since the films with n in the range 3–5 typically result in significantly higher photoluminescence quantum yield (PLQY) compared to other compositions.[4,7] In addition, we have selected hexylammonium (HA) as a spacer cation, since HA-based 2D perovskites exhibit the highest out-of-plane mobility and the lowest self-trapped exciton emission among the alkyl chain spacer cations.[38] This is attributed to the fact that both the interlayer distance and spacer cation conformational disorder affect the mobility and broadband emission, resulting in nonlinear dependence on the alkyl chain length.[38] While the same behavior in terms of observed trends in crystal structure and optical properties holds for other spacer cations, such as BA and octylammonium (OA), obtained efficiency of HA-based devices is significantly higher.

© 2021 Wiley-VCH GmbH

2. Results and Discussion

Figure 1a,b shows the absorption and photoluminescence (PL) spectra of $HA_2(Cs_xFA_{1-x})_{n-1}Pb_nBr_{3n+1}$ prepared with $n = 4$ stoichiometry for different Cs content x. We can observe significant differences in the absorption spectra of the films shown in Figure 1a (vertical lines indicate positions of excitonic peaks corresponding to different n phases). FA-only films exhibit prominent peaks due to different n phases for $n = 2$, 3, 4, etc., which is in agreement with a previous work that reports pronounced absorption peaks corresponding to low n phases in the case of FA-only samples.[10] As the fraction of FA reduces, the absorption peaks corresponding to different n phases of quasi-2D perovskite are reduced, while the absorption spectrum of the sample corresponding to Cs-only sample does not show evidence of quasi-2D phases. All the films exhibit green emission peak only, and a shift in the emission peak center is observed with increasing FA content (from 513 nm for Cs-only to 534 nm for FA-only), as shown in **Figure 2**c. However, while films show a consistent and continuous shift in optical properties, a pronounced difference in the performance of LED as function of FA content is observed, with the maximum efficiency significantly enhanced for the Cs:FA ratio of 1:1. The schematic diagrams of the LED and the corresponding energy levels are shown in Figure S1, Supporting Information, and the energy levels determined from the ultraviolet photoelectron spectroscopy (UPS) measurements are also summarized in Table S1, Supporting Information. Electroluminescence (EL) spectra of the device with $HA_2(Cs_{0.5}FA_{0.5})_{n-1}Pb_nBr_{3n+1}$ active layer for different bias voltages are shown in Figure 1c, while the EL spectra of the devices for additional Cs:FA ratios are shown in Figure S2, Supporting Information. Similar to the PL spectra, the emission maximum exhibits redshift with increasing FA content. We can also observe shoulders corresponding to lower n phase emissions for pure FA devices, which likely contributes to their lower efficiency due to inefficient energy transfer. The performance of the devices for different Cs content x is summarized in Table S2 (Supporting Information). EQE histograms for devices consisting of $HA_2(Cs_xFA_{1-x})_3Pb_4Br_{13}$ with $x = 0$, 0.5, and 1 are shown in Figure 1d, while the EQE histograms for additional compositions $x = 0.25$ and 0.75 are given in Figure S3, Supporting Information. Dramatic enhancement in the performance of $HA_2(Cs_{0.5}FA_{0.5})_{n-1}Pb_nBr_{3n+1}$ devices is observed compared to those with other Cs:FA ratios. The obtained

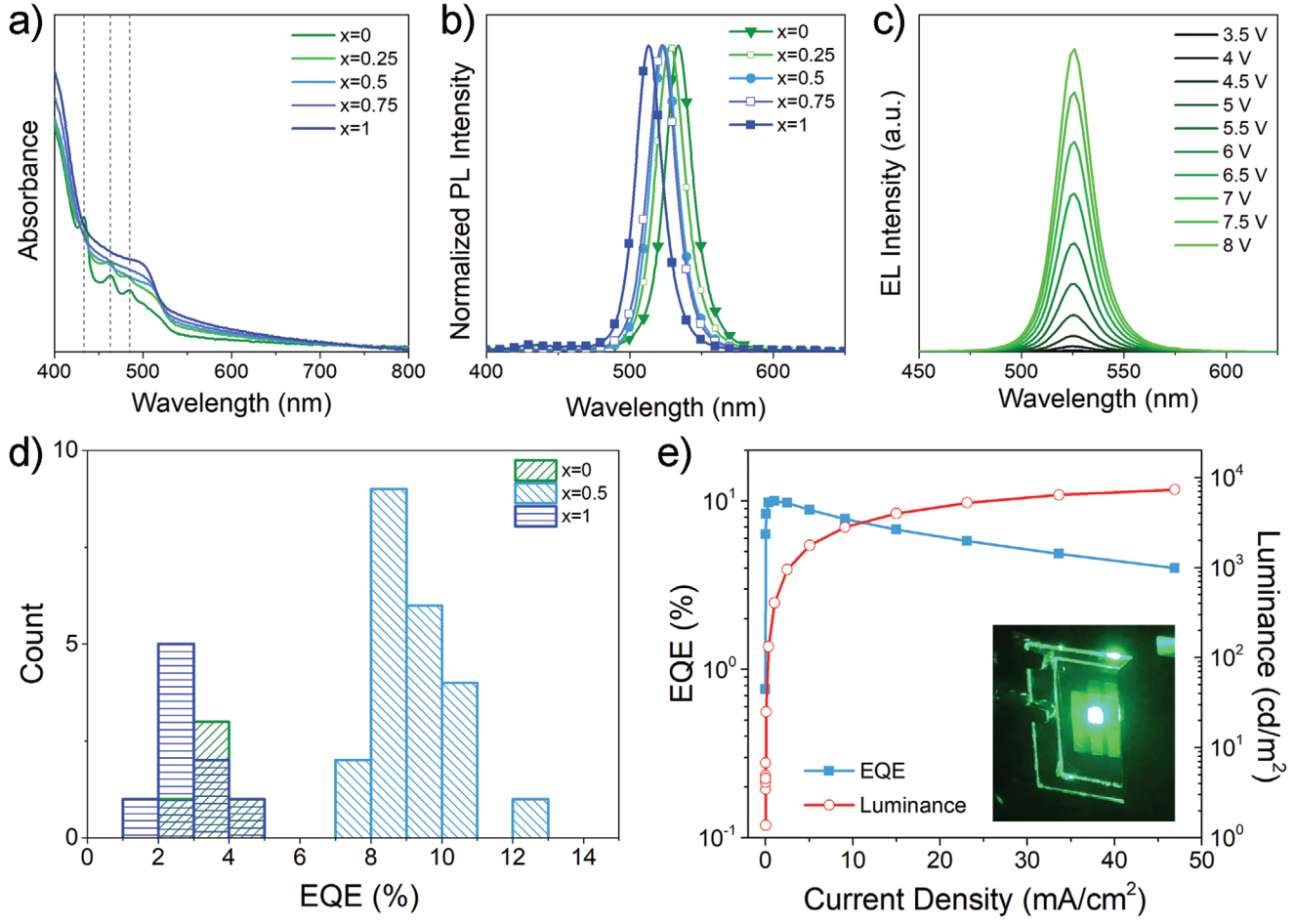

Figure 1. a) Absorption and b) normalized PL spectra of $HA_2(Cs_xFA_{1-x})_{n-1}Pb_nBr_{3n+1}$ films with different Cs content x. c) EL spectra of $HA_2(Cs_{0.5}FA_{0.5})_{n-1}Pb_nBr_{3n+1}$ based LED device as a function of bias voltage. d) EQE histograms of $HA_2(Cs_xFA_{1-x})_{n-1}Pb_nBr_{3n+1}$ based LED devices with $x = 0$, 0.5, and 1. e) Luminance and EQE of the best $HA_2(Cs_{0.5}FA_{0.5})_{n-1}Pb_nBr_{3n+1}$ based device as a function of current density. Photo of the device is shown in the inset. All the perovskite films were prepared with solution stoichiometry corresponding to $n = 4$.

© 2021 Wiley-VCH GmbH

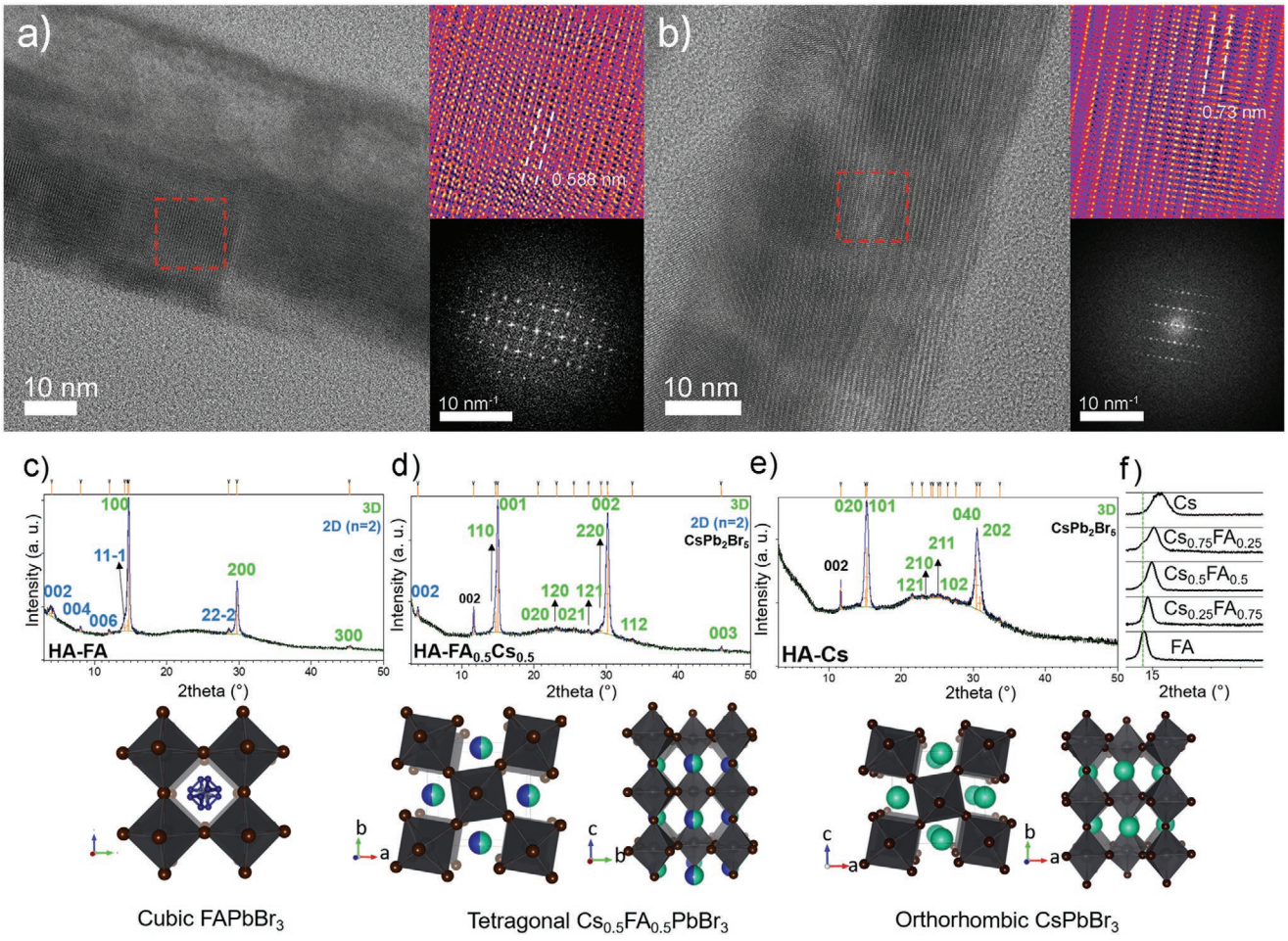

Figure 2. a,b) TEM and HRTEM images of $HA_2(Cs_{0.5}FA_{0.5})_{n-1}Pb_nBr_{3n+1}$ films prepared with $n = 4$ stoichiometry, showing 3D and $n = 2$ domains. c–f) XRD patterns of $HA_2(Cs_xFA_{1-x})_{n-1}Pb_nBr_{3n+1}$ films for $x = 0$, 0.5, and 1. Miller indices of 3D reflections ($APbBr_3$) are given in green while those belonging to $HA_2(A)Pb_2Br_7$ and $CsPb_2Br_5$ are given in blue and black, respectively.

maximum EQE of 12.1%, maximum current eficiency of 46.1 cd A^{-1}, and maximum luminance of 15 070 cd m^{-2} compare favorably to the literature reports on the performance of quasi-2D perovskite-based green LEDs (summarized in Table S3, Supporting Information), since our devices, in a large majority of cases, outperform those reported in the literature in at least one of the three performance parameters (EQE, current efficiency, or maximum luminance). It was previously reported that devices exhibited reduced efficiency roll-off when mixed small cations are used,[10,14,19] and the use of mixed cations was also reported to result in longer device lifetimes compared to Cs-only devices[14] and FA only devices.[19] However, here we do not observe significant differences in the EQE dependence on current bias for devices with mixed small cations (Figure 1e) and single small cation devices (Figure S4, Supporting Information). The lifetime of the devices with optimal composition is shown in Figure S5 (Supporting Information), for two different initial bias values. The T_{50} corresponding to initial luminance of 100 cd m^{-2} is 32 min, while longer lifetime of 1.83 h is obtained at lower bias.

Understanding the reasons behind such a significant increase in efficiency and maximum luminance (2–3 times) for $HA_2(Cs_{0.5}FA_{0.5})_{n-1}Pb_nBr_{3n+1}$, compared to other compositions with different Cs and FA contents, is particularly important in order to identify the crucial factors that have led to remarkable improvement of device performance. Therefore, we performed comprehensive investigations of the film structure and optical properties, in comparison with the perovskites prepared with Cs only and FA only. For the sake of consistency all optical and structural measurements have been performed on the films prepared on poly[(9,9-dioctylfluorenyl-2,7-diyl)-alt-(4,4′-(N-(4-butylphenyl) (TFB) thin film, or complete devices in the case of transmission electron microscopy (TEM) investigations, since the film morphology and the absorption considerably depend on the type of substrates, as shown in Figure S6, Supporting Information.

From the TEM images of the devices (Figure 2a,b), we can observe that the mixed films consist of small crystals in a disordered matrix. It has been previously reported that in situ formation of nanocrystals can improve light emission from halide perovskite films, which was attributed to a reduction in nonradiative recombination due to nanocrystal surface passivation,[15,16,18] and that amorphous lead bromide ammonium complexes located at the surface can be responsible for the

© 2021 Wiley-VCH GmbH

luminescence of $CsPb_2Br_5$.[36] No such formation of nanocrystals was observed in single small cation films, as shown in Figure S7, Supporting Information. Furthermore, from the HRTEM images shown in Figure 2, we can identify the presence of a 3D phase (001 at d = 5.88 Å) and a quasi-2D n = 2 phase (012 at d = 7.3 Å), and we also observe the presence of 3D phase in single cation samples (Figure S7, Supporting Information).

The presence of 3D phase and quasi-2D n = 2 phase, evident from the absorption spectra and HRTEM, is additionally confirmed by the XRDdata. Despite the fact that thin films have been prepared from solutions corresponding to n = 4 stoichiometry, X-ray diffraction (XRD) analysis revealed dominant presence of 3D perovskite structure ($APbBr_3$) in all samples, regardless of the choice and ratio of A cation(s). Figure 2c–e shows XRD patterns of perovskites obtained by using HA as the spacer cation, while FA, $Cs_{0.5}FA_{0.5}$, and Cs as A-site cations, respectively. XRD patterns for the samples having other compositions at A site including $Cs_{0.25}FA_{0.75}$ and $Cs_{0.75}FA_{0.25}$, are shown in Figure S8, Supporting Information.

In the case when A-site is occupied exclusively by FA cations (Figure 2c), the 3D phase exhibits only h00 reflections and it was indexed assuming cubic symmetry with a unit cell parameter a = 5.991(2) Å, in accordance with literature data.[23] Additional Bragg reflections belonging to 3D phase appeared with decreasing amount of FA cations on A site indicating the tetragonal distortion with the increase in Cs content (Figure 2d). In the case of $Cs_{0.5}FA_{0.5}PbBr_3$, the decrease in symmetry becomes evident from the appearance of 110 and 220 reflections at left-hand side of major 00l reflections, at 14.66° and 29.67° respectively, as well as from low intensity lines that can be seen from the enlarged region 20°–30° in the XRD pattern (Figure S9, Supporting Information). We can observe that, in addition to the reflections at ≈20.5° (which can be indexed as tetragonal 020 or cubic 011) and at ≈25.5° (which could be indexed as tetragonal 021 or cubic 111), there are additional reflections at ≈22.9° and 27.5° which correspond to tetragonal 120 and 121 reflections, respectively, and which could not appear in a cubic cell. The structure of $Cs_{0.5}FA_{0.5}PbBr_3$ has been refined in the tetragonal P4/mbm space group with the unit-cell parameters $a = b$ = 8.642(2) Å and c = 5.922(3) Å. Refined lattice parameters are smaller compared to the reported similar iodine-based structure,[39] due to a smaller ionic radius of bromide.

Although experimental XRD patterns exhibit several features that clearly indicate the symmetry lowering in the case of $Cs_{0.5}FA_{0.5}PbBr_3$, density functional theory (DFT) calculations were exploited to gain further insight into the stability of several possible structures, assuming both tetragonal, and cubic lattices. As shown in **Figure 3**, seven possible arrangements of A-cations (four within cubic and three within tetragonal lattice) have been studied.

Indeed, DFT calculations show that tetragonal lattices of $Cs_{0.5}FA_{0.5}PbBr_3$ are slightly more stable compared to the cubic structures. Also, it was realized that the structure containing stacks of the same type of cations along c-direction is more stable compared to the arrangements having layers of the same type cation in ab plane or those having Cs and FA in alternating zig-zag layers in ab plane. However, the relative energy difference between different assemblies (layered, alternated zig-zag, aligned) all lies within 1.2 kcal mol^{-1} which is less than 2 kT, suggesting that all of the arrangements might easily form in the real samples.

In the case when A-site is occupied by Cs cations exclusively, a further symmetry lowering can be noted from XRD patterns (Figure 2e); it is primarily manifested as a diffraction profile broadening and by the appearance of additional broad low intensity reflections, therefore a full pattern decomposition fitting was performed assuming the orthorhombic symmetry. The structure of $CsPbBr_3$ crystallizes in Pnma space group, adopting a distorted perovskite structure with octahedra tilted with respect to the orthogonal geometry of the ideal perovskite lattice, with the refined unit-cell parameters a = 8.248(1) Å, b = 11.726(2) Å, c = 8.161(2) Å which is in an accordance with a structure determined by Kanatzidis et al.[40] While the diffraction lines ≈23° (d≈3.86) and ≈25.5 °(d≈3.49), indexed in orthorhombic cell as 210 and 211, could have also be indexed in

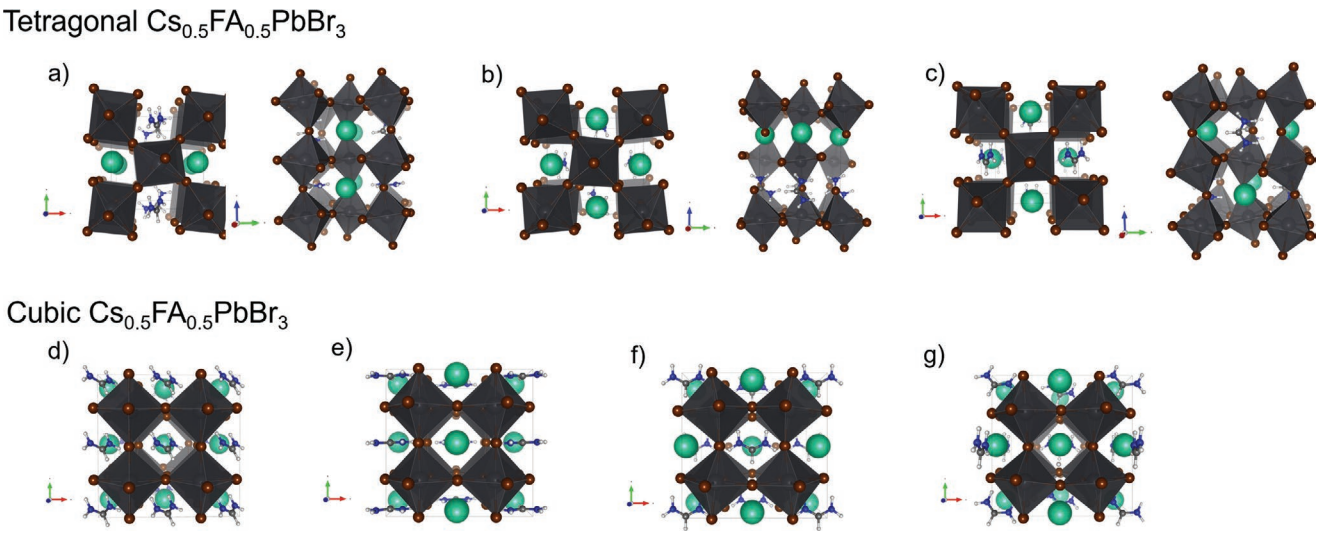

Figure 3. Possible arrangements of A cations in tetragonal and cubic $Cs_{0.5}FA_{0.5}PbBr_3$.

© 2021 Wiley-VCH GmbH

higher tetragonal symmetry as 120 and 021, respectively, the rest of the reflections in the range from 24.4° to 26.5° (such as 201, 031, 022) cannot be present in the cubic nor tetragonal symmetry. Thus, their appearance in XRD pattern conclusively confirms the orthorhombic symmetry. Figure 2f shows that the diffraction line positions are shifted to higher 2θ positions as the Cs molar proportion in the $FA_{1-x}Cs_xPbBr_3$ films increased due to the difference in radius sizes of A-site cations ($r(Cs^+) = 1.81$ Å, $r(FA^+) = 2.79$ Å). The gradual shift of diffraction line positions also confirms the presence of solid solution without phase segregation in the whole range of compositions, in agreement with a previous report.[14] We also evaluated formation energy relative to precursor compounds of each 3D perovskite and found that it is the highest for $FAPbBr_3$, while mixed $Cs_{0.5}FA_{0.5}PbBr_3$ is more favorable by 3.4 kcal mol^{-1} and pure $CsPbBr_3$ by 10.9 kcal mol^{-1}. Besides these internal energies evaluated by DFT, it should be noted that mixing cations additionally gives rise to entropic contribution to stabilization.[41]

XRD analysis also shows that the dominant presence of 3D perovskite phase is accompanied by some amount of 2D perovskite ($n = 2$) phase and layered $CsPb_2Br_5$ phase (except in the cases of FA-based samples). $CsPb_2Br_5$ phase has been identified based on structure as reported by Huang et al.[42] The reflections belonging to $HA_2FAPb_2Br_7$ ($n = 2$) structure have been indexed according to similar iodine-based compound $HA_2MAPb_2I_7$.[43] As expected the crystal lattice of $HA_2FAPb_2Br_7$ exhibits a smaller periodicity along c-direction (002 at $d = 22.02$ Å) compared to $HA_2MAPb_2I_7$ (002 at $d = 22.37$ Å) due to the fact that Br^- radius is smaller than I^- (even though FA is slightly larger compared to MA). Similar to 3D phase, diffraction lines belonging to RP $n = 2$ phase exhibit gradual shift of 00l reflections as a function of Cs:FA ratio; 002 line of $HA_2FAPb_2Br_7$ shifts from 22.02 to 21.56 Å for $HA_2Cs_{0.5}FA_{0.5}Pb_2Br_7$ due to the partial incorporation of Cs^+ instead of FA^+. The fact that thin films, although being prepared from solutions corresponding to $n = 4$ stoichiometry, contain a mixture of 3D phase and some amount of low-dimensional phase, has additionally been addressed by DFT. The DFT calculations show, although the energy difference is quite small, that the mixture of 3D perovskite and $n = 2$ phase has 0.5 kcal mol^{-1} lower energy compared to the pure $n = 4$ phase.

The grazing-incidence wide angle x-ray scattering (GIWAXS) results shown in **Figure 4** are in excellent agreement with the phases found in the XRD patterns. In addition, the GIWAXS

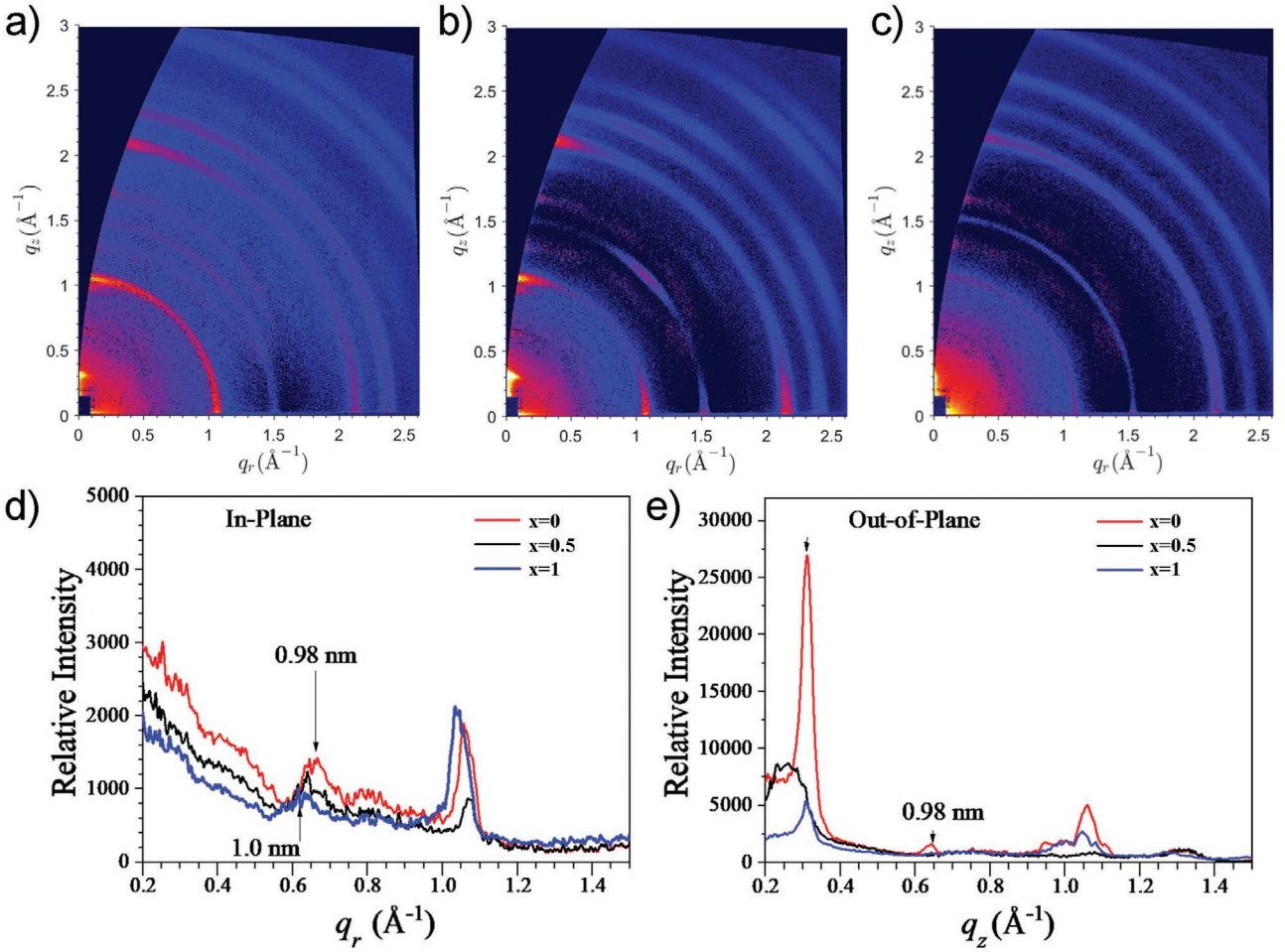

Figure 4. GIWAXS 2D patterns for $HA_2(Cs_xFA_{1-x})_{n-1}Pb_nBr_{3n+1}$ films for: a) $x = 0$, b) $x = 0.5$, and c) $x = 1$. d,e) Integrated in-plane and out-of-plane 1D profiles for $HA_2(Cs_xFA_{1-x})_{n-1}Pb_nBr_{3n+1}$ films for different Cs:FA ratio. Note the highly oriented layering peak along the film-normal direction (z) of the CsFA mixing case. All the perovskite films were prepared with solution stoichiometry corresponding to $n = 4$.

© 2021 Wiley-VCH GmbH

scattering arcs, rather than X-ray diffraction powder ring, observed for the mixed sample indicate highly oriented perovskite crystals along the out-of-plane direction of the film, as shown in Figure 4e. Moreover, the GIWAXS data reveal an additional highly oriented peak centered at $q_z = 0.29$ Å^{-1} (Figure 4e), revealing a layer structure of 2D perovskite of a *d*-spacing of 2.16 nm oriented along the film normal direction. Such a layering direction is parallel to the [110] planes of the 3D perovskite crystal structure observed both in GIWAXS and consistently in the XRD. These results suggest that the coexisting 2D and 3D perovskites are particularly orientation-aligned in the mixed sample.

It has been noted that the reflection corresponding to *d*-spacing ≈1.0 nm appears also in the "small spacer cation" type of RP $n = 1$ perovskite structures where small guanidinium (GA) cations, typically present exclusively within the octahedral voids, act as spacer cations.[44] Similarly in our case, we might expect the formation of such a special type of RP phase with Cs or FA cations acting as very small spacer cations. Indeed, all-inorganic Ruddlesden–Popper phases $Cs_{n+1}Pb_nBr_{3n+1}$ have been previously observed in HRTEM,[45] while similarly they could not be detected in XRD, but the structure details have not been reported. However, since according to GIWAXS data, this phase is present in all samples, it likely does not contribute to the observed light-emitting performance differences and therefore investigation of its formation and properties is beyond the scope of this work.

The transient absorption spectroscopy is commonly used to investigate energy transfer in quasi-2D perovskite films.[2,5] From the transient absorption measurements, shown in **Figure 5**, we observe high energy peaks at ≈460 and ≈480 nm which we attribute as the bleaching of the transitions in the lower *n* phases, well aligned with the high energy absorption peak positions in Figure 1a. A large peak at ≈515 nm, aligned with the absorption band edge, is rapidly populated (the high energy peaks disappear by 10 ps, as shown in Figure S10, Supporting Information) and slowly decays by 1 ns. The TA spectra probed at > 200 ps show no presence of the high energy peaks likely due to highly efficient energy transfer between different phases (from lower *n* toward 3D). Furthermore, this indicates that the presence of quasi-2D perovskites, even at low amounts, still play a significant role in the light emission from the samples. The presence of lower *n* phases is also obvious from the extinction coefficient of the samples determined by spectroscopic ellipsometry, shown in Figure S11, Supporting Information.

Time-resolved photoluminescence (TRPL) characterization was performed to investigate the carrier dynamics and recombination of $HA_2(Cs_{1-x}FA_{0x})_{n-1}Pb_nBr_{3n+1}$ thin films for $x = 0$, 0.5, and 1.0 as shown in Figure S12, Supporting Information.

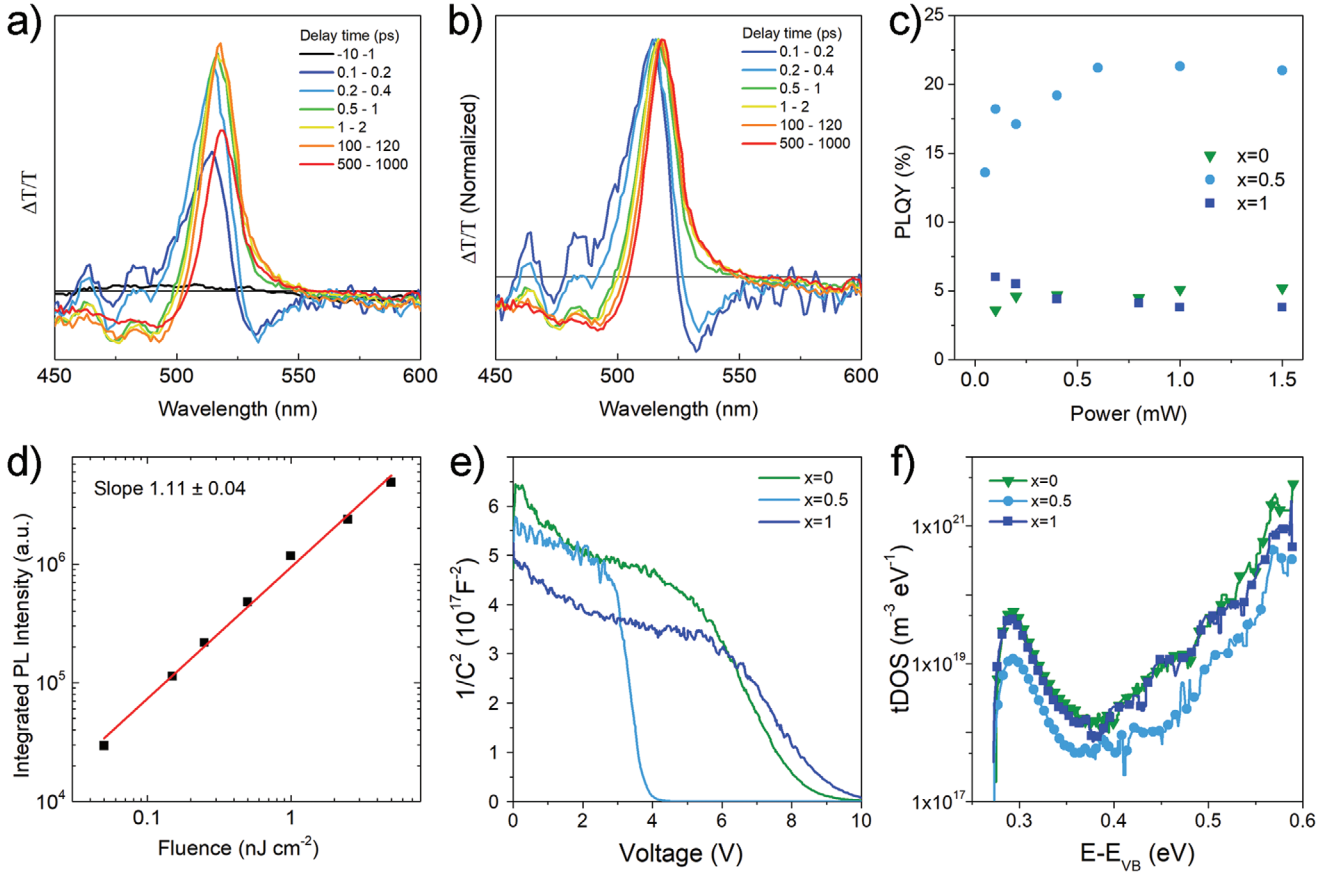

Figure 5. a,b) Transient absorption spectra, c) PLQY, and d) integrated PL intensity as a function of excitation power of HA_2 $(Cs_{0.5}$ $FA_{0.5})_{n-1}Pb_nBr_{3n+1}$ thin film. e) Mott–Schottky plot and f) tDOS of $HA_2(Cs_xFA_{1-x})_{n-1}Pb_nBr_{3n+1}$ based LED devices. All the perovskite films were prepared with solution stoichiometry corresponding to $n = 4$.

© 2021 Wiley-VCH GmbH

Obtained decay curves can be fitted by a biexponential function. The decay of $x = 0$ and $x = 1$ samples show clearly two distinct components, whereas the $x = 0.5$ sample shows an overall longer decay lifetime. Biexponential fittings have been used to characterize perovskite films, where the fast decay component is related to recombination of surface or trap states, and the longer lifetime component results from radiative decay.[46,47] The fast component in $x = 0$, 0.5, and 1, are 1.54, 3.68, 1.59, with weight fractions of 0.62, 0.60, 0.64, respectively, suggesting that the $x = 0$ and 1 samples may have increased trap or surface states.

Biexponential weighted average lifetimes of $\tau_{avg} = 9.4$ ns for $x = 0.5$, $\tau_{avg} = 4.5$ ns for $x = 0$, and $\tau_{avg} = 7.4$ ns for $x = 1$ indicate the higher optical quality of the $x = 0.5$ film, possibly related to the suppression of nonradiative decay. To gain additional insight into the radiative recombination, we calculate the rates of radiative recombination of the three samples by taking the average lifetimes of the $x = 0$, 0.5, and 1.0 and comparing it to the measured PLQY.[48,49] Obtained rates are given in Table S4, Supporting Information. The observed reduction in nonradiative recombination rate for $x = 0.5$ sample is in agreement with increased PLQY of $x = 0.5$ sample, as shown in Figure 5c.

From the obtained PLQY, we can observe significant difference between $HA_2(Cs_{0.5}FA_{0.5})_{n-1}Pb_nBr_{3n+1}$, exhibiting a maximum PLQY of 21.3%, and $HA_2FA_{n-1}Pb_nBr_{3n+1}$ and $HA_2Cs_{n-1}Pb_nBr_{3n+1}$ which exhibit maximum PLQY values of 5.4% and 6%, respectively. The decreased lifetime and lower PLQY for samples having Cs content $x = 1.0$ and 0 are attributed to an increase in nonradiative recombination, possibly due to a difference in defect trapping originating from specific structural, but also microstructural, features found for the mixed cation phase compared to those of single cations. It should be noted that these PLQY values are external PLQY values measured for surrogate thin films on a given substrate, as opposed to actual active layers in a working device. Accordingly, their direct interpretation is limited by differences in outcoupling, that depend on sample structure, and thus they are not equal to internal quantum yield. However, information on the refractive indices, thickness, and external PLQY can be used to estimate the escape probability following a previously reported procedure[50] briefly summarized in the Supporting Information. Within these considerations, the internal quantum yield, corresponding to externally measured maximum PLQY of 21.3%, is estimated to be in the range 45–55% as shown in Table S5, Supporting Information, which is in good agreement with the LED performance. It should also be noted that these are rough estimates which can be further complicated by the fact that exact sample structure affects not only the outcoupling, but also by the fact that the layers deposited below or above the perovskite can affect the interfacial trap density, resulting in mismatch between PLQY of films and EQE of the devices. This is experimentally illustrated in Figures S13 and S14, Supporting Information, showing the difference in the light emission of perovskite films on different substrates with and without TPBi layer on top of the perovskite. We have also investigated if small cation mixing has a general positive effect on light emission. For this, we prepared nanocrystals in solution (using hexylamine as a ligand) and obtained significant PLQY enhancement for $x = 0.5$ (PLQY = 52.6%), which is much higher than for FA- or Cs-only samples, with PLQY = 31.7% and PLQY = 3.6%, respectively. The $x = 0.5$ and $x = 1$ samples also clearly showed the presence of tetragonal and orthorhombic structures, respectively, as shown in Figure S15, Supporting Information. While the magnitude of enhancement achieved for mixed cation samples compared to FA-only and Cs-only cations differs in thin films and nanocrystals, as expected from differences in the synthesis procedures, it is obvious that the FA:Cs 1:1 ratio still yields significantly higher enhancement of light emission.

Finally, considering that our samples dominantly contain 3D perovskites, it is necessary to examine the nature of the radiative recombination. It is known that the integrated PL intensity I_{PL} is described by the power law of the excitation power density I_{ex}, $I_{PL} \approx I_{ex}^{k}$, where $k = 2$ corresponds to free carrier recombination, $1 < k < 2$ corresponds to excitonic recombination, and $k < 1$ indicates involvement of defects (free-to-bound exciton and donor–acceptor recombination).[17] The obtained slope of $k = 1.11+0.04$ is in good agreement with a previous report on exciton localization in 3D perovskites ($k = 1.179$).[17] Similar linear dependences are obtained for $HA_2FA_{n-1}Pb_nBr_{3n+1}$ and $HA_2Cs_{n-1}Pb_nBr_{3n+1}$. We note that the PL line shape as well as the peak energy does not change for the different excitation intensities. It should also be noted that defect emissions and/or self-trapped excitons in perovskites are typically associated with broad emissions (FWHM ≈80 nm) and long PL lifetimes (μs range), while here we observe the PL lifetimes in ns range and narrow emission peaks, which is consistent with the obtained results confirming excitonic recombination. However, it should be noted that these measurements were performed using a femtosecond pulse laser, which results in fast creation of high carrier densities. In the case of PLQY measurement performed using a continuous wave laser diode, we can observe a decrease in PLQY for very low power for $x = 0.5$ samples, which is consistent with trap filling. Nevertheless, for excitation densities for the TRPL measurements, all three samples are in the linear regime corresponding to flat PLQY response in the PLQY power dependence.

Thus, based on the optical and structural investigations, we can conclude that the use of mixed small cations results in a significant alteration of crystallization of the perovskite films, resulting not only in the suppression of the formation of large n phases observed for pure FA-based samples, but also in the suppression of formation of large crystal domains, observed in pure Cs-based samples. The Cs:FA 1:1 mixed films consist of small crystals in disordered matrix which probably passivate the surface defects and result in improved radiative recombination efficiency. It has been previously proposed that Cs-FA mixed cation perovskite films had fewer traps compared to pure Cs-based perovskite,[22] but trap densities were not measured. To examine the defect densities in the films, we have performed capacitance-voltage measurements, and the resulting Mott–Schottky plot is shown in Figure 5e. The trap density of states (tDOS) of perovskite-based LED devices as shown in Figure 5f, was obtained according to the methods reported in the literature.[52] Depletion width (W) and built-in potential (V_{bi}) were calculated from Mott–Schottky measurement at 1 kHz, and the perovskite films were fully depleted. The Attempt-to-escape

© 2021 Wiley-VCH GmbH

frequency ω_0 was assumed to be 10^{12} s^{-1} so that the frequency was converted into energy scale via the following equation[52]

$$E_\omega = k_B T \ln \frac{\omega_0}{\omega} \quad (1)$$

Thus tDOS was calculated by

$$N_T(E_\omega) = -\frac{V_{bi}}{qW}\frac{dC_p}{d\omega}\frac{\omega}{k_B T} \quad (2)$$

where q, k_BT, C_p and ω are electron charge, thermal energy, capacitance, and angular frequency. From the obtained results, we can observe that the built-in potential and the trap density in the mixed small cation films are considerably lower compared to FA- and Cs-based samples. The reduction of the trap density would result in a reduction of nonradiative recombination losses,[52] in agreement with the observed enhancement of PLQY and LED performance. Furthermore, we can observe a reduction in the trap density both in deep traps corresponding to surface/interface defects, as well as shallow traps corresponding to defects in the perovskite film (grain boundaries).[53,54]

It should also be noted that the observed behavior applies not only to the perovskites with HA spacer cations, but also to the perovskites with other alkyl chain spacer cations. Absorption and PL spectra of the films with different Cs/FA content with BA and OA spacer cations are shown in Figures S16 and S17, Supporting Information, respectively, while the corresponding GIWAXS patterns and XRD patterns are shown in Figures S18–S20, Supporting Information. However, obtained device performances are considerably lower, with the maximum EQE of 0.02% and current efficiency of 0.07 cd A^{-1} for BA-based devices, and maximum EQE of 1.73% and current efficiency 6.81 cd A^{-1} for OA-based devices. This is likely due to the superior optical and charge transport properties of HA-based perovskites, which represents an optimal length of the alkyl chain spacer taking into account both chain length and its conformational disorder.[38]

3. Conclusion

This work demonstrates that by controlling the ratio of small cations Cs and FA, we can tailor the crystallization processes occurring in perovskite thin films and thus tune the specific structural and microstructural features of crystalline phases. The optimal ratio of Cs:FA of 1:1 leads to the formation of preferentially grown tetragonal $Cs_{0.5}FA_{0.5}PbBr_3$ phase that exhibits reduced trap density (compared to FA-only and Cs-only samples) and finally results in significant enhancement of PLQY from 5% to 6% for single cation samples up to 21.3% for $Cs_{0.5}FA_{0.5}$-based samples. The LED performance is similarly enhanced, with mixed cation devices exhibiting a maximum EQE of 12.1%, maximum luminance of 15 070 cd m^{-2} and maximum current efficiency of 46.1 cd A^{-1}, which is significantly higher than that of single cation devices which exhibit EQE of ≈4% and maximum luminance below 5000 cd m^{-2}.

Supporting Information

Supporting Information is available from the Wiley Online Library or from the author.

Acknowledgements

This work was supported by the Seed Funding for Basic Research and Seed Funding for Strategic Interdisciplinary Research Scheme of the University of Hong Kong, RGC GRF Project Nos. 17301520 and 11210218, RGC CRF Project No. 7035-20G, NSFC Project Nos. 62075187, and PZS-2019-02-2068 project financed by the "Research Cooperability" Program of the Croatian Science Foundation funded by the European Union from the European Social Fund under the Operational Programme Efficient Human Resources 2014–2020, and The Shenzhen Fundamental Research Program (No. JCYJ20170412154447469). The authors would like to thank Dr. K. H. Low (Chemistry, HKU) for performing XRD measurements.

Conflict of Interest

The authors declare no conflict of interest.

Author Contributions

F.Z.L. and X.S.Q. conducted the experiments of synthesizing perovskite materials, fabrication of perovskite-based LED devices, as well as characterization of absorption and steady state photoluminescence. M.G. and B.H. conducted high-resolution TEM characterization of perovskite samples and related data analysis. C.C.S.C., C.M., and K.S.W. conducted measurements of photoluminescence quantum yield, time-resolved photoluminescence, temperature dependent photoluminescence, transient absorption, and related data analysis. T.L.L. conducted the capacitance-voltage measurements and Mott–Schottky analysis of perovskite-based LED devices, while W.C. performed encapsulation and device lifetime tests. Y.L.H. and A.M.C.N. performed X-ray diffraction and ultraviolet photoelectron spectroscopy analysis of the perovskite samples. S.W. performed PLQY measurement of nanocrystal samples. M.R.H. and J.A.Z. conducted ellipsometry measurements of selected perovskite samples and related data analysis. Y.L.S. and F.C.C.L. conducted frequency dependent capacitance measurement. C.J.S. and U.-S.J. conducted GIWAXS analysis of the perovskite samples. I.L., L.G., J.O., conducted DFT simulations. J.P. and Ž.S. conducted structural analysis of perovskite samples. J.P. contributed to the writing of the manuscript. A.D. designed the whole investigation, analyzed the corresponding results, and contributed to the writing of the manuscript.

Data Availability Statement

Research data are not shared.

Keywords

green emission, perovskite light-emitting diodes, quasi-2D perovskites, Ruddlesden–Popper, X-ray diffraction

Received: February 24, 2021
Revised: June 20, 2021
Published online: August 20, 2021

© 2021 Wiley-VCH GmbH

[1] F. Zhang, H. Lu, J. Tong, J. J. Berry, M. C. Beard, K. Zhu, *Energy Environ. Sci.* **2020**, *13*, 1154.
[2] W. Cha, H. Han, Y. Hong, G. Kim, C. Park, D. Kim, *J. Phys. Chem. C* **2020**, *124*, 4414.
[3] M. U. Ali, J. Miao, J. Cai, D. F. Perepichka, H. Yang, H. Meng, *ACS Appl. Mater. Interfaces* **2020**, *12*, 18761.
[4] M. Yuan, L. N. Quan, R. Comin, G. Walters, R. Sabatini, O. Voznyy, S. Hoogland, Y. Zhao, E. M. Beauregard, P. Kanjanaboos, Z. Lu, D. H. Kim, E. H. Sargent, *Nat. Nanotechnol.* **2016**, *11*, 872.
[5] L. N. Quan, Y. Zhao, F. P. Garcia de Arquer, R. Sabatini, G. Walters, O. Voznyy, R. Comin, Y. Li, J. Z. Fan, H. Tan, J. Pan, M. Yuan, O. M. Bakr, Z. Lu, D. H. Kim, E. H. Sargent, *Nano Lett.* **2017**, *17*, 3701.
[6] T. Cheng, C. Qin, S. Watanabe, T. Matsushima, C. Adachi, *Adv. Funct. Mater.* **2020**, *30*, 2001816.
[7] X. Yang, X. Zhang, J. Deng, Z. Chu, Q. Jiang, J. Meng, P. Wang, L. Zhang, Z. Yin, J. You, *Nat. Commun.* **2018**, *9*, 570.
[8] Z. Wang, F. Wang, W. Sun, R. Ni, S. Hu, J. Liu, B. Zhang, A. Alsaed, T. Hayat, Z. A. Tan, *Adv. Funct. Mater.* **2018**, *28*, 1804187.
[9] M. You, H. Wang, F. Cao, C. Zhang, T. Zhang, L. Kong, L. Wang, D. Zhao, J. Zhang, X. Yang, *ACS Appl. Mater. Interfaces* **2020**, *12*, 43018.
[10] T. Wu, Y. Yang, Y. Zou, Y. Wang, C. Wu, Y. Han, T. Song, Q. Zhang, X. Gao, B. Sun, *Nanoscale* **2018**, *10*, 19322.
[11] P. Vashishtha, M. Ng, S. B. Shivarudraiah, J. E. Halpert, *Chem. Mater.* **2019**, *31*, 83.
[12] F. Meng, X. Liu, Y. Chen, X. Cai, M. Li, T. Shi, Z. Chen, D. Chen, H. L. Yip, C. Ramanan, P. W. M. Blom, S. J. Su, *Adv. Funct. Mater.* **2020**, *30*, 1910167.
[13] J. Yan, G. Croes, A. Fakharuddin, W. Song, P. Heremans, H. Chen, W. Qiu, *Adv. Opt. Mater.* **2019**, *7*, 1900465.
[14] M. Yang, N. Wang, S. Zhang, W. Zou, Y. He, Y. Wei, M. Xu, J. Wang, W. Huang, *J. Phys. Chem. Lett.* **2018**, *9*, 2038.
[15] F. Liu, C. C. S. Chan, C. Ma, H. W. Tam, T. L. Leung, J. Lin, A. B. Djurišić, K. S. Wong, J. Popović, A. M. C. Ng, W. K. Chan, W. Chen, Z. He, A. E. Adesina, Y. Foo, J. A. Zapien, *Adv. Opt. Mater.* **2019**, *7*, 1900269.
[16] L. Zhao, Y. W. Yeh, N. L. Tran, F. Wu, Z. Xiao, R. A. Kerner, Y. L. Lin, G. D. Scholes, N. Yao, B. P. Rand, *ACS Nano* **2017**, *11*, 3957.
[17] H. He, Q. Yu, H. Li, J. Li, J. Si, Y. Jin, N. Wang, J. Wang, J. He, X. Wang, *Nat. Commun.* **2016**, *7*, 10896.
[18] Z. Xiao, R. A. Kerner, L. Zhao, N. L. Tran, K. Lee, T. W. Koh, G. D. Scholes, B. P. Rand, *Nat. Photonics* **2017**, *11*, 108.
[19] G. Yang, X. Liu, Y. Sun, C. Teng, Y. Wang, S. Zhang, H. Zhou, *Nanoscale* **2020**, *12*, 1571.
[20] Z. Xiao, Q. Wang, X. Wu, Y. Wu, J. Ren, Z. Xiong, X. Yang, *Org. Electron.* **2020**, *77*, 105546.
[21] F. Ye, H. Zhang, P. Wang, W. Li, D. Li, B. Du, D. Liu, T. Wang, *ACS Appl. Mater. Interfaces* **2019**, *11*, 43452.
[22] G. Xie, C. Jiang, J. Wang, C. Mai, G. Huang, Y. Ma, J. Wang, J. Peng, Y. Cao, *Org. Electron.* **2019**, *71*, 58.
[23] H. Cho, J. S. Kim, C. Wolf, Y. H. Kim, H. J. Yun, S. H. Jeong, A. Sadhanala, V. Venugopalan, J. W. Choi, C. L. Lee, R. H. Friend, T. W. Lee, *ACS Nano* **2018**, *12*, 2883.
[24] X. Zhang, H. Liu, W. Wang, J. Zhang, B. Xu, K. L. Karen, Y. Zheng, S. Liu, S. Chen, K. Wang, X. W. Sun, *Adv. Mater.* **2017**, *29*, 1606405.
[25] B. Xu, W. Wang, X. Zhang, W. Cao, D. Wu, S. Liu, H. Dai, S. Chen, K. Wang, X. Sun, *J. Mater. Chem. C* **2017**, *5*, 6123.
[26] J. Si, Y. Liu, N. Wang, M. Xu, J. Li, H. He, J. Wang, Y. Jin, *Nano Res.* **2017**, *10*, 1329.
[27] J. Dai, Y. Fu, L. H. Manger, M. T. Rea, L. Hwang, R. H. Goldsmith, S. Jin, *J. Phys. Chem. Lett.* **2016**, *7*, 5036.
[28] X. Zhang, B. Xu, J. Zhang, Y. Gao, Y. Zheng, K. Wang, X. W. Sun, *Adv. Funct. Mater.* **2016**, *26*, 4595.
[29] C. Qin, T. Matsushima, A. S. D. Sandanayaka, Y. Tsuchiya, C. Adachi, *J. Phys. Chem. Lett.* **2017**, *8*, 5415.
[30] Z. P. Huang, B. Ma, H. Wang, N. Li, R. T. Liu, Z. Q. Zhang, X. D. Zhang, J. H. Zhao, P. Z. Zheng, Q. Wang, H. L. Zhang, *J. Phys. Chem. Lett.* **2020**, *11*, 6007.
[31] B.-S. Zhu, H.-Z. Li, J. Ge, H.-D. Li, Y.-C. Yin, K.-H. Wang, C. Chen, J.-S. Yao, Q. Zhang, H.-B. Yao, *Nanoscale* **2018**, *10*, 19262.
[32] M. Cao, Y. Damji, C. Zhang, L. Wu, Q. Zhong, P. Li, D. Yang, Y. Xu, Q. Zhang, *Small Methods* **2020**, *4*, 2000303.
[33] S. K. Balakrishnan, P. V. Kamat, *Chem. Mater.* **2018**, *30*, 74.
[34] S. Caicedo-Dávila, R. Gunder, J. A. Márquez, S. Levcenko, K. Schwarzburg, T. Unold, D. Abou-Ras, *J. Phys. Chem. C* **2020**, *124*, 19514.
[35] T. Zhang, Z. Chen, Y. Shi, Q. H. Xu, *Nanoscale* **2019**, *11*, 3186.
[36] P. Acharyya, P. Pal, P. K. Samanta, A. Sarkar, S. K. Pati, K. Biswas, *Nanoscale* **2019**, *11*, 4001.
[37] Y. B. Cheng, Q. H. Sun, P. Zhang, F. B. Wang, B. B. Zhang, G. D. Zhang, W. Q. Jie, Y. D. Xu, *J. Phys. Chem. Lett.* **2020**, *11*, 5625.
[38] C. Z. Li, J. Yang, F. H. Su, J. J. Tan, Y. Luo, S. J. Ye, *Nat. Commun.* **2020**, *11*, 5481.
[39] J. A. Vigil, A. Hazarika, J. M. Luther, M. F. Toney, *ACS Energy Lett.* **2020**, *5*, 2475.
[40] C. C. Stoumpos, C. D. Malliakas, J. A. Peters, Z. Liu, M. Sebastian, J. Im, T. C. Chasapis, A. C. Wibowo, D. Y. Chung, A. J. Freeman, B. W. Wessels, M. G. Kanatzidis, *Cryst. Growth Des.* **2013**, *13*, 2722.
[41] C. Y. Yi, J. S. Luo, S. Meloni, A. Boziki, N. Ashari-Astani, C. Grätzel, S. M. Zakeeruddin, U. Röthlisberger, M. Grätzel, *Energy Environ. Sci.* **2016**, *9*, 656.
[42] Z. Zhang, Y. Zhu, W. Wang, W. Zheng, R. Lin, F. Huang, *J. Mater. Chem. C* **2018**, *6*, 446.
[43] I. Spanopoulos, I. Hadar, W. Ke, Q. Tu, M. Chen, H. Tsai, Y. He, G. Shekhawat, V. P. Dravid, M. R. Wasielewski, A. D. Mohite, C. C. Stoumpos, M. G. Kanatzidis, *J. Am. Chem. Soc.* **2019**, *141*, 5518.
[44] O. Nazarenko, M. R. Kotyrba, S. Yakunin, M. Wörle, B. M. Benin, G. Rainó, F. Krumeich, M. Kepenekian, J. Even, C. Katan, M. V. Kovalenko, *Chem. Mater.* **2019**, *31*, 2121.
[45] Y. Yu, D. D. Zhang, P. D. Yang, *Nano Lett.* **2017**, *17*, 5489.
[46] P. W. Liang, C. Y. Liao, C. C. Chueh, F. Zuo, S. T. Williams, X. K. Xin, J. J. Lin, A. K. Y. Jen, *Adv. Mater.* **2014**, *26*, 3748.
[47] A. H. Slavney, T. Hu, A. M. Lindenberg, H. I. Karunadasa, *J. Am. Chem. Soc.* **2016**, *138*, 2138.
[48] N. Droseros, G. Longo, J. C. Brauer, M. Sessolo, H. J. Bolink, N. Banerji, *ACS Energy Lett.* **2018**, *3*, 1458.
[49] D. K. Sharma, S. Hirata, L. Bujak, T. Kameyama, V. Biju, M. Kishi, T. Torimoto, M. Vacha, *Phys. Chem. Chem. Phys* **2017**, *19*, 3963.
[50] J. M. Richter, M. Abdi-Jalebi, A. Sadhanala, M. Tabachnyk, J. P. H. Rivett, L. M. Pazos-Outón, K. C. Gödel, M. Price, R. H. Friend, F. Deschler, *Nat. Commun.* **2016**, *7*, 13941.
[51] P. Nandi, C. Giri, D. Topwal, *J. Mater. Chem. C* **2021**, *9*, 2793.
[52] J. Byun, H. Cho, C. Wolf, M. Jang, A. Sadhanala, R. H. Friend, H. Yang, T.-W. Lee, *Adv. Mater.* **2016**, *28*, 7515.
[53] X. Zhang, J. Zhang, D. Phuyal, J. Du, L. Tian, V. A. Öberg, M. B. Johansson, U. B. Cappel, O. Karis, J. Liu, H. Rensmo, G. Boschloo, E. M. J. Johansson, *Adv. Energy Mater.* **2018**, *8*, 1702049.
[54] Z. Ni, C. X. Bao, Y. Liu, W. Q. Wu, S. S. Chen, X. Z. Dai, B. Chen, B. Hartweg, Z. S. Yu, Z. Holman, J. S. Huang, *Science* **2020**, *367*, 1352.

© 2021 Wiley-VCH GmbH